Energy Storage Flywheel Magnetic Bearing System – Magnetic Linear Circuit vs. 3-D Finite Element Model

Arunvel Kailasan[a], Tim Dimond[b], Paul Allaire[c]

[a] Gardner Denver, Inc., 100 Gardner Park, Peachtree City, GA 30269, USA, arunvel.kailasan@gardnerdenver.com
[b] Rotor Bearing Solutions International, 3277 Arbor Trace, Charlottesville, VA 22911, USA, tim.dimond@rotorsolution.com
[c] Rotor Bearing Solutions International, 3277 Arbor Trace, Charlottesville, VA 22911, USA, paul.allaire@rotorsolution.com

***Abstract*—A 1 kW-hr (3.6 MJ) energy storage flywheel with a design operating speed of 40,000 rpm and an inside-out flywheel has been designed and optimized. It is supported in two thrust and two radial active magnetic bearings. The purpose of this paper is to present the active magnetic bearing system modeling including the magnetic analysis.**

At the design stage, there are two ways to evaluate the magnetic bearing properties: linear circuit model or finite element model. The linear circuit models are simple lumped mass models. The finite element model discretizes the bearing geometry and the surrounding space and requires a great deal more work. There are not many full 3-D finite element magnetic bearing systems that have been fully compared to the equivalent linear circuit model. There are legitimate questions about accuracy of magnetic bearing modeling results.

This paper considers these two approaches to compare the results for a realistic energy storage flywheel design. If the differences are large, it is expected that the 3-D finite element model is more likely to be accurate. This paper documents the differences for the flywheel magnetic bearing designs.

The linear circuit model prediction of axial force capacity was 17% lower and the prediction of coil indcutance was 8% lower than the predictions from 3-D finite element model. The linear circuit model of the radial bearing underestimated the force capacity by 14% and underestimated the inductance by 8.5% when compared to the 3D finite element model. Values were also compared for the open loop stiffness, current gain and force slew rate for both bearing designs.

These relatively large differences in magnetic bearing performance parameters obtained between the linear circuit model and the 3-D finite element model, shows that the linear circuit model is not very accurate. Thus, the concern is that designing and optimizing a complex magnetic bearing supported device requires 3-D finite element modeling at the design stage.

The flywheel has not been constructed and the magnetic bearings are thus not available for testing. It is hoped that this can be future work.

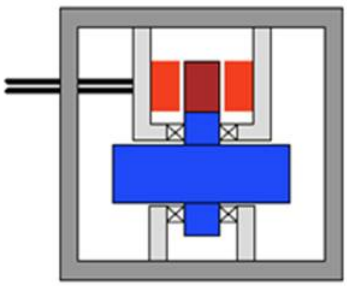

(a) Conventional Schematic

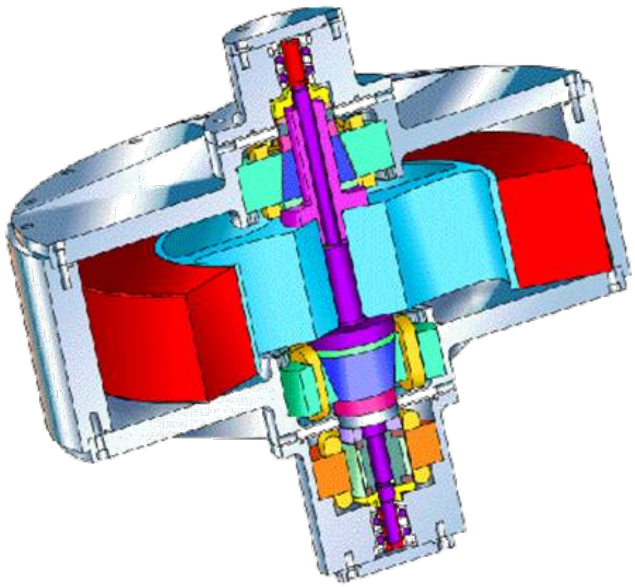

(b) Conventional Example

Figure 1: Conventional Flywheel Design

I. Introduction

Active magnetic bearings have advantages over traditional rolling-element or fluid film bearing designs. Active magnetic bearing systems have significantly lower power losses than fluid film bearing systems and allow for effective system damping, unlike rigidly-mounted rolling element bearing systems. As a results, AMBs are an enabling technology for efficient high-speed flywheel design. When combined with a vacuum chamber, parasitic losses resulting from flywheel rotation are minimized. The design of the magnetic bearing system is therefore an integral part of having a good, highly efficient flywheel design.

There are two basic design configurations of flywheel sys-

tems commercially available: a conventional design and an integrated design. In the "conventional design," the rotor has a large diameter section, where most of the kinetic energy is stored, attached to a smaller diameter section, which is used by the motor to spin the flywheel. This is the most common design. However, this configuration tends to have a larger housing and containment structure because of the additional rotor length. This results in a very heavy flywheel configuration which can be expensive to manufacture. A schematic of the conventional configuration is shown in Fig. 1a. A generic conventional flywheel design is shown in Fig. 1b.

The second configuration is an "integrated design" in which the electromagnetic and energy storage portions of the rotor are combined. This type of design is found in newer generation flywheels but is not well suited for composite rotor flywheels because of the need for electromagnetic material for torque production. However, in the integrated configuration, the housing and stator of the motor comprise a large portion of the vacuum and burst containment for the flywheel. A typical 1kW-hr integrated flywheel weighs about 200 -250 Kg. A schematic of the integrated design is shown in Fig. 2a and the integrated design from Active Power [1] is shown in Fig. 2b.

A variant of the integrated flywheel is the barrel type flywheel, shown schematically in Fig. 3a. An example barrel configuration flywheel design from PowerTHRU (formerly Pentadyne) [2] is shown in Fig. 3b. This design variant places the electromagnetic parts of the rotor on the inner diameter of the rotor. With this configuration, the outer diametral portion of the rotor can be either steel or composite material for energy storage.

At the design stage, the magnetic bearing properties can be determined either with linear circuit models or with finite element analysis. Jang et al. [3] used linear circuit models to develop initial design parameters for thrust AMBs, including thrust load, coil resistance, and coil inductance. The designs were confirmed with finite element analysis and experiment.

Jang et al. [4] introduced fringing correction factors into a linear circuit model of an active magnetic thrust bearing to improve load predictions. Results were compared to a finite element analysis and experiment. Permeance correction factors based on bearing geometry were developed from analysis. These correction factors brought the circuit model into agreement with the finite element model within 1% and also closely tracked experimental measurements. The uncorrected linear circuit model underpredicted the thrust load both as a function of position and as a function of current.

Zhang and Tian [5] developed an analytical expression for eddy current losses in active magnetic thrust bearings. The magnetic diffusion equations were solved for a non-laminated thrust bearing and compared to a finite element analysis. The two analyses gave identical results for frequencies up to 1 kHz, and were within 10% for frequencies from 1 kHz-10 kHz.

The flywheel design for this study is a barrel-type design, shown schematically in Fig. 4. The 5-axis AMB system for the flywheel is comprised of a double-acting thrust bearing and two radial magnetic bearings. The double acting thrust bearing system is a normal AMB with one coil and two poles in the upper and lower bearings. A linear magnetic circuit

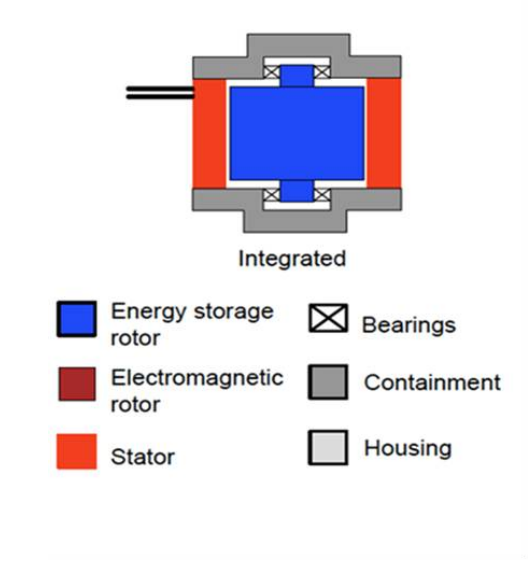

(a) Integrated Schematic

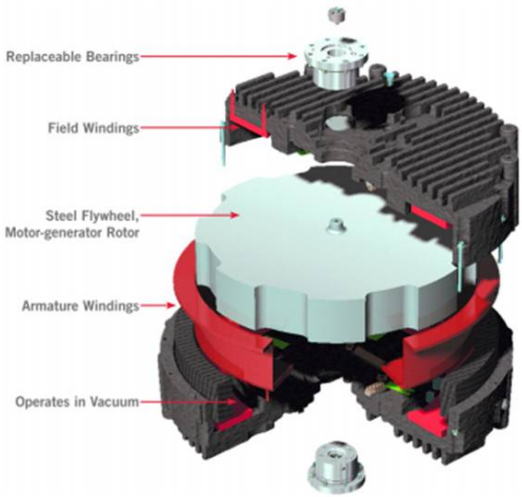

(b) Integrated Example - Active Power Flywheel [1]

Figure 2: Integrated Flywheel Design Example

for the thrust bearing is used to determine the magnetic flux density, magnetic pole forces, the inductance, the open loop stiffness, the current and the slew rate for a given coil current. The linear magnetic circuit values obtained are compared to a full 3-D analysis of the same geometry thrust bearing.

The radial bearings were designed as inside-out operating bearings with the rotor on the outside and the stator on the inside. They had twelve poles in an E-core design. The radial force capability, inductance, open loop stiffness, current gain and force slew rate were all evaluated using a linear circuit model and a 3-D finite element model using a similar procedure to the thrust bearing analysis.

II. Active Magnetic Bearings

The bearing analysis was conducted in two parts. The initial designs were obtained assuming linear magnetic circuit theory. Peak magnetic fluxes were limited to ensure that the linearity

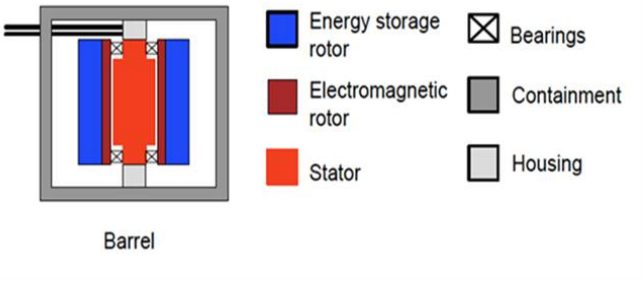

(a) Barrel Schematic

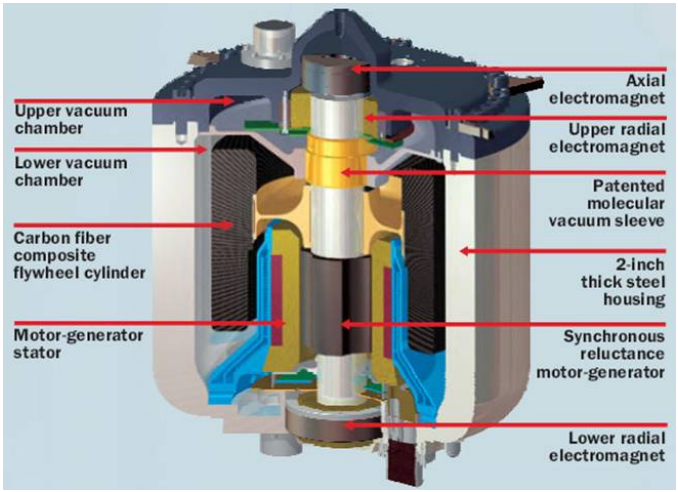

(b) Barrel Example - PowerTHRU Flywheel [2]

Figure 3: Barrel Flywheel Design Example

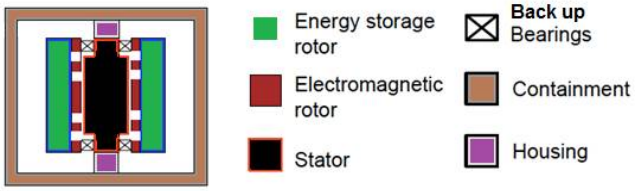

Figure 4: Integrated Flywheel Design, Present Study

assumption remained valid. The design flux density at the knee of the curve was taken as 1.2 T. This is a typical linear B-H flux limit for silicon iron alloys. A packing factor of 0.7 was applied in computing the coil cavity dimensions and the amount of copper wire available to energize the bearing. The packing factor accounts for unused space with round wire winding and wire insulation. The packing factor results in an increased packing volume when calculating the magnetic bearing size. A 14 AWG wire was used for the analysis.

Then, the results of the linear analyses were confirmed using non-linear finite element analysis (FEA) performed with a commercial code. The FEA included saturation effects in the magnetic materials.

A. Linear Circuit Models

The equations for the linear magnetic circuit models presented are available in [3]. The fundamental equations for magnetic circuit analysis are Ampere's loop law and conservation of magnetic flux. Ampere's loop law describes the induced magnetic field due to an applied current in a wire coiled around magnetic material and is given by

$$\sum_{i=1}^{n_i}\left(\frac{Bg}{\mu_0}\right)_i = \sum_{i=1}^{n_i}(NI)_i \tag{1}$$

where B is the magnetic flux density, g is the nominal air gap, μ_0 is the permitivitty of free space, $4\pi\cdot 10^{-7}$ H/m, N is the number of winding turns, and I is the input current in A. Conservation of magnetic flux indicates that the total flux Φ_i through a node in the magnetic circuit is zero:

$$\sum_{i=1}^{n_i}\Phi_i = 0 \tag{2}$$

The available force $\mathbf{f}$ was obtained in terms of the peak magnetic flux density B_{sat} for a lumped model as:

$$\mathbf{f} = \frac{A_p B_{sat}^2}{2\mu_0}\mathbf{n} \tag{3}$$

The vector $\mathbf{n}$ is a unit normal to the pole face area A_p. The maximum available pole face area was limited by the back iron cross-sectional area and the stator inner and outer diameters. The back iron was sized to saturate at the same input current density as the poles.

The slew rate magnitude was calculated in terms of linearized bearing operation for opposing pairs of the AMB designs in the circuit models as

$$\frac{d\,|\mathbf{f}|}{dt} = \frac{\mu_0 A_p N^2 I_b}{2g}\frac{dI_p}{dt} \tag{4}$$

where I_b is the bias current and I_p is the perturbation current. The rate of change of perturbation current is limited by the open-loop inductance L and the peak amplifier voltage V_c as

$$\frac{dI_p}{dt} = \frac{V_c}{L} \tag{5}$$

To properly design the bearing controller, the open loop characteristics of the bearings are needed to characterize the plant. The open loop stiffness is found as

$$k_x \approx -\frac{\partial\,|\mathbf{f}|}{\partial x}\bigg|_{x=x_0, i_p=i_{p_0}} \tag{6}$$

The open loop stiffness is negative, indicating that AMBs are open-loop unstable.

The current gain for the bearing is found as

$$k_i \approx \frac{\partial\,|\mathbf{f}|}{\partial i_p}\bigg|_{x=x_0, i_p=i_{p_0}} \tag{7}$$

B. Finite Element Analysis

Results for a three-dimensional finite element analysis performed using commercial finite element software were compared to the bearing design parameters obtained from the linear circuit models. The dimensions of the initial bearing size using the linear circuit models described in Section II-A is presented in Kailasan [6]. The magnetic flux paths was determined for both the thrust and radial magnetic bearings, and important

parameters such as load capacity, flux density, inductance, magnetic field energy and slew rate were calculated.

The finite elements implement the fundamental constitutive electromagnetic relations in a discretized form. The fundamental relationships are a subset of Maxwell's equations and include magnetomotance, given by

$$\nabla \times \mathbf{H} = \mathbf{J} \tag{8}$$

where **H** is the magnetic field intensity and and **J** is the current density.

The conservation of magnetic flux **B** at a given cross-sectional area in the bearing in differential form is expressed as:

$$\nabla \cdot \mathbf{B} = 0 \tag{9}$$

The applied force from the magnetic fields developed in the AMB and directed through the air gaps is given by

$$\mathbf{f} = \oint \mathbf{T} \cdot d\mathbf{S} \tag{10}$$

The term **T** in (10) is the Maxwell stress tensor, expressed using indicial notation as

$$T_{ij} = \frac{1}{\mu_0}\left(B_i B_j - \frac{1}{2}\delta_{ij} B_{ij}^2\right) \tag{11}$$

where δ_{ij} is the Kronecker delta.

Coil inductance is not directly available from the finite element solution. However, the inductance can be found from the total magnetic field energy produced by the maximum current. The inductance can then be calculated as [7]:

$$L_c = \frac{2W}{I^2} \tag{12}$$

where L_c is the inductance in H, W is the magnetic field energy in J, and I is the current applied to the magnetic bearing coils in A.

C. Thrust Bearing

A double-acting thrust magnetic bearing was designed for the flywheel. The section view of the thrust magnetic bearing is shown in Fig. 5. With a vertical rotor orientation, the main function of the thrust bearing is to support the entire flywheel mass and to resist dynamic thrust loads while in operation. The bearing consists of three major parts: the thrust disk, which is the rotating part of the bearing and is attached to the flywheel, the thrust stator which is attached to the stator back iron, and the coils inside the stator.

A three dimensional finite element analysis using commercial software was conducted to verify the parameters obtained from the linear circuit model of the thrust bearing. A mesh density study was performed to ensure that the results had numerically converged. About 1 million elements were used in the analysis, with a denser mesh in the air gap to improve accuracy. Figure 6 shows the modeled thrust magnetic bearing.

The flux path and the maximum load capacity were calculated with maximum current applied to the coils. Other parameters of interest are the inductance, slew rate and magnetic field energy. The finite element method allows for modeling

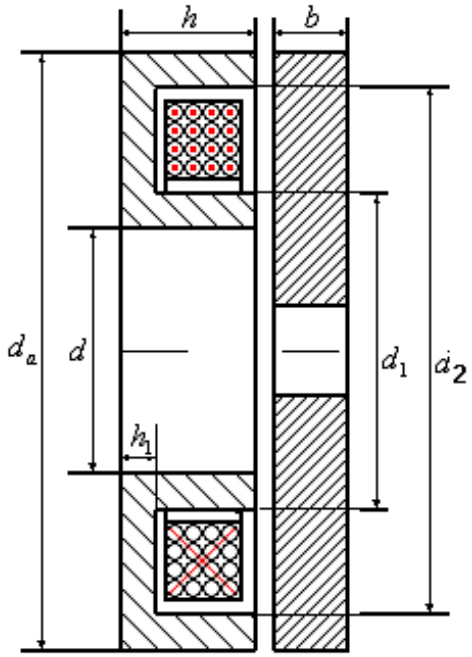

Figure 5: Thrust AMB

of flux leakage and is more accurate than linear circuit models that assume all flux is in the air gap.

To calculate the value of open loop stiffness, the rotor was centered between the opposing thrust magnets while applying equal currents to each coil, resulting in zero net force. The rotor was then moved axially in increments of 0.05 mm, and a force versus displacement curve was calculated based on five increments. The slope of the line gives the open loop stiffness k_x.

The current gain was obtained by varying the value of the perturbation current with the rotor centered axially in the model and plotting net force versus perturbation current. The slope of the line for force versus perturbation current gives the current gain k_i.

D. Radial Bearings

The inside-out rotor design with the stator in the center required an innovative inside-out E-core type radial magnetic bearing design for the flywheel, as shown in Fig. 7. In contrast to traditional magnetic bearing designs, the bearing consists of an inner laminated stator component and an outer rotor lamination stack. The stator poles are pointed radially outwards as shown in Fig. 7. The stator component is attached to the stator core while the laminations are attached to the inner steel spline rotor.

In this design, the rotating part of the bearing is the outer ring. The bearing poles, windings, and the back iron are inside of the rotating ring and are on the stator. The 12-pole E-core arrangement has four quadrants. The main pole in the center of each quadrant has about twice the pole face area as the two auxiliary poles.

As with the case of the thrust bearing, a 3-D FEA was conducted to compare results for the load capacity, flux path and

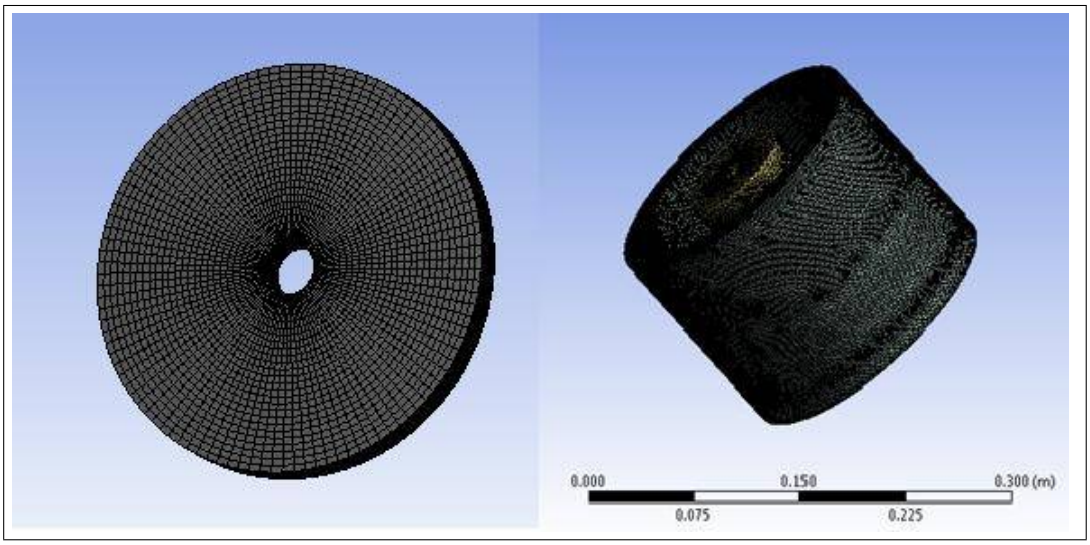

Figure 6: 3D Thrust AMB Finite Element Mesh

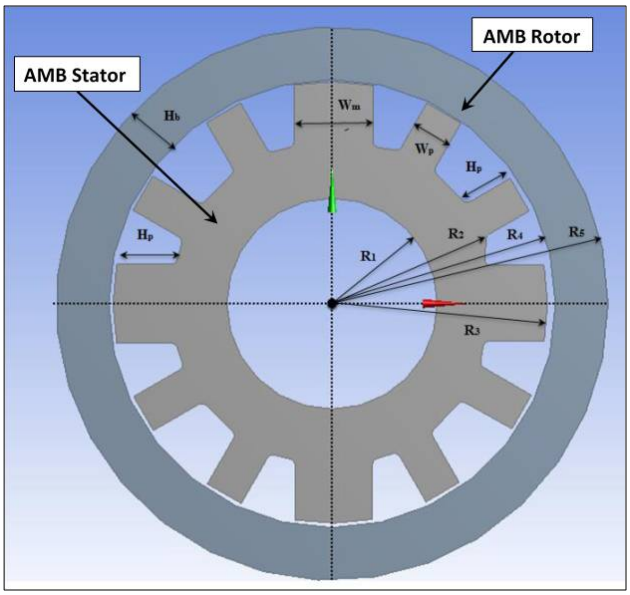

Figure 7: Radial AMB Inverted Design

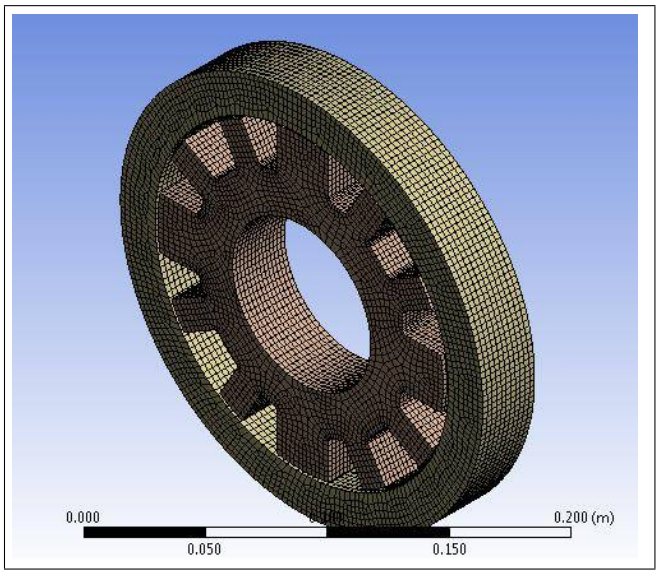

Figure 8: Radial AMB Finite Element Mesh

flux density while calculating parameters such as inductance, magnetic energy and slew rate. The location and extent of magnetic saturation was also evaluated with the finite element analysis. The E-core model is shown in Fig. 8. A similar perturbation procedure to that used for the thrust bearing was used to determine open loop stiffness k_x and current gain k_i. The inductance was computed based on Eq. (12).

III. Results

A. Thrust Magnetic Bearing

Table I shows a comparison between the linear circuit model and the 3-D FEA values obtained for the flywheel thrust bearing. A sample thrust bearing flux density finite element solution is shown in Fig. 9. The peak calculated load capacity from the FEA was 1800 N. This was 17% larger than load capacity of 1500 N calculated using the linear circuit model. The inductance predicted by the finite element model was 9% higher than what was predicted by the linear circuit model. This led to a corresponding decrease in force slew rate predicted by the finite element model when compared to the linear circuit model.

Differences were also found in the predictions of actuator open-loop characteristics. When compared to the finite element model, the linear circuit model overpredicted open loop stiffness magnitude by 19% and underpredicted current gain by 4.2%. While there is a large difference in predicted open loop stiffness, this large a difference can be treated as an uncertainty in modern control methods such as H_∞ or μ-synthesis.

The linear circuit model also overpredicted slew rate by 21% when compared to the 3-D FEA. Since slew rate is a linear function of coil inductance, this was to be expected.

Table I: Thrust Bearing Design Values

Property	Value	
	Linear Circuit Model	3D FEA
F_{max}, N	1500	1812
W, J	-	3.82
L_c, mH	68.1	74.5
k_x N/mm	-172.1	-143.9
k_i N/A	286.6	299
Slew, N/s	$3.9{\cdot}10^6$	$3.2{\cdot}10^6$

Table II: Radial Bearing Design Values

Property	Value	
	Linear Circuit Model	FEA
F_{max}, N	850	990
W, J	-	4.68
L_c, mH	92.4	101.2
k_x N/mm	-128.3	-113.4
k_i N/A	42.6	45.3
Slew, N/s	$7.1{\cdot}10^6$	$6.4{\cdot}10^6$

However, it is an indication that the linear circuit model is overly optimistic in estimating the ability of the magnetic bearing to react to rapid changes in force.

The peak magnetic flux obtained from the finite element model was about 1.24 T. Equal and opposite forces were found on the thrust disk and the stator, indicating that the analysis had converged. There was strong agreement between the peak flux in the 3-D FEA and the 1.2 T peak flux assumed in the linear circuit model for design purposes.

B. Radial Magnetic Bearing

As with the thrust bearing, a 3-D finite element model was made for comparison to the results obtained from a linear circuit model. A mesh convergence study was done to performed to ensure that the analysis had numerically converged. About 1 million elements were used for the analysis. An example flux density solution from the radial bearing finite element model is shown in Fig. 10.

A summary of the FEA results compared to the values obtained from linear circuit models is presented in Table II. The maximum load capacity from the 3-D FEA was 990 N. This was 16% higher than the 850 N obtained from the linear circuit model. As with the thrust bearing, the inductance predicted by the radial bearing finite element model was about 9% higher than that predicted by the linear circuit model.

As with the thrust bearing, there were significant differences in the actuator open-loop characteristics between the 3-D FEA and the linear circuit model. When compared to the FEA, the linear circuit model prediction for open loop stiffness magnitude was 13% higher. The linear circuit model prediction for current gain was 6% lower than the FEA prediction.

The slew rate prediction from the linear circuit model was 11% higher than the 3-D FEA prediction for the radial bearing. This is consistent with the difference in prediction for the inductance for this bearing.

The FEA predicted a peak flux of 1.36 T, which is entering the saturation flux region of silicon iron alloys. This may account for some of the difference in load capacity between the FEA and the linear circuit model, since magnetic flux was limited to 1.2 T in the linear circuit model.

IV. Conclusions

In this paper, linear circuit models for an active magnetic thrust bearing and an active magnetic radial bearing were compared to 3D finite element models. A consistent finding from both analyses was that the finite element analysis consistently predicted higher load capacity than was found using linear circuit models. This was surprising, since the linear circuit model treated magnetic components as ideal lumped parameters. It is expected that fringing and leakage effects would have served to reduce the load capacity since some of the magnetic flux is not used to generate force. However, this finding was consistent with the findings of Jang et al. [4]. Another possibility is that the calculated peak flux from the FEA was higher than the assumed peak flux from the linear circuit models. The peak flux in the linear circuit model is set at 1.2T. In the finite element model, calculated peak flux was as high as 1.34 T. This additional flux would result in increased force and may also part of the difference between the linear circuit models and the FEA.

The finite element prediction for current gain was up to 19% higher than the prediction from the linear circuit model for the current gain. While this is a large difference, it should be manageable since there is some model reconciliation that is part of the initial levitation process. Similar comments apply to the difference in open loop stiffness between models. While an underestimate of the open loop stiffness could result in an unstable closed-loop system if the control gain is too low, this should be able to be corrected during initial levitation.

Some of these differences between linear circuit models and finite element analysis can be mitigated by using derating factors on the linear design equations to account for fringing and leakage effects, as shown by Jang et al. [4]. However, these derating factors must be empirically confirmed. The FEA accounts for fringing, leakage, and non-linearity effects and is easier to verify.

Based on these results, linear circuit models are suitable for preliminary sizing of AMB actuators and for quickly iterating on design options. The final design and final actuator size should be based on the finite element analysis.

References

[1] Active Power, "Active Power CleanSource UPS Multi-Module Systems," Downloaded from `http://www.activepower.com/Documents/Datasheets/CSMMS-US-W.pdf` on 15 June 2014.

[2] "Pentadyne's VSSDC," *Broadcast Engineering*, vol. 48, no. 9, pp. 90–92, 2006.

[3] S.-M. Jang, U.-H. Lee, J.-Y. Choi, and J.-P. Hong, "Design and analysis of thrust active magnetic bearing," *Journal of Applied Physics*, vol. 103, no. 7, pp. 07F122–07F122, 2008.

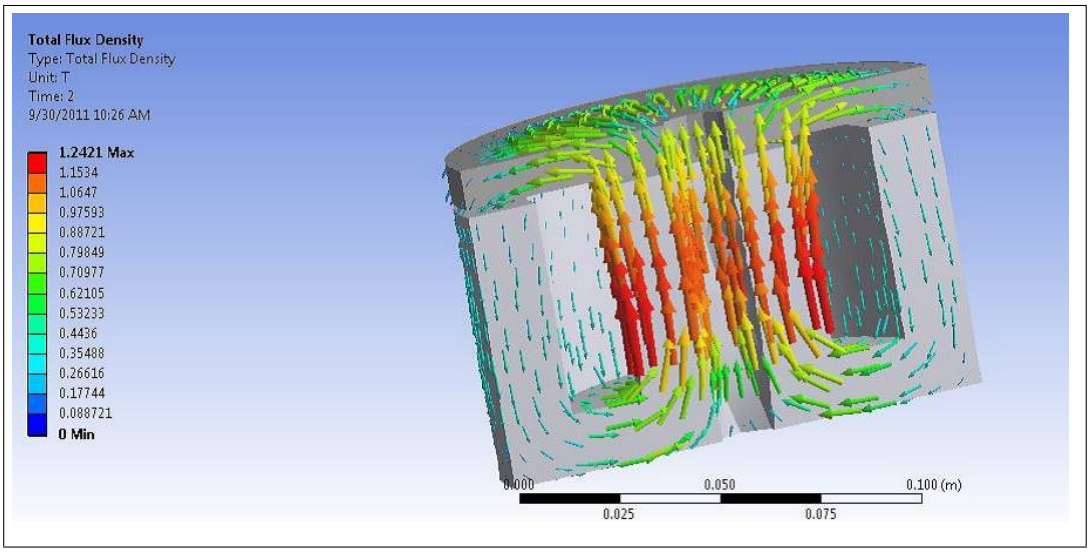

Figure 9: 3D Thrust AMB Finite Element Analysis

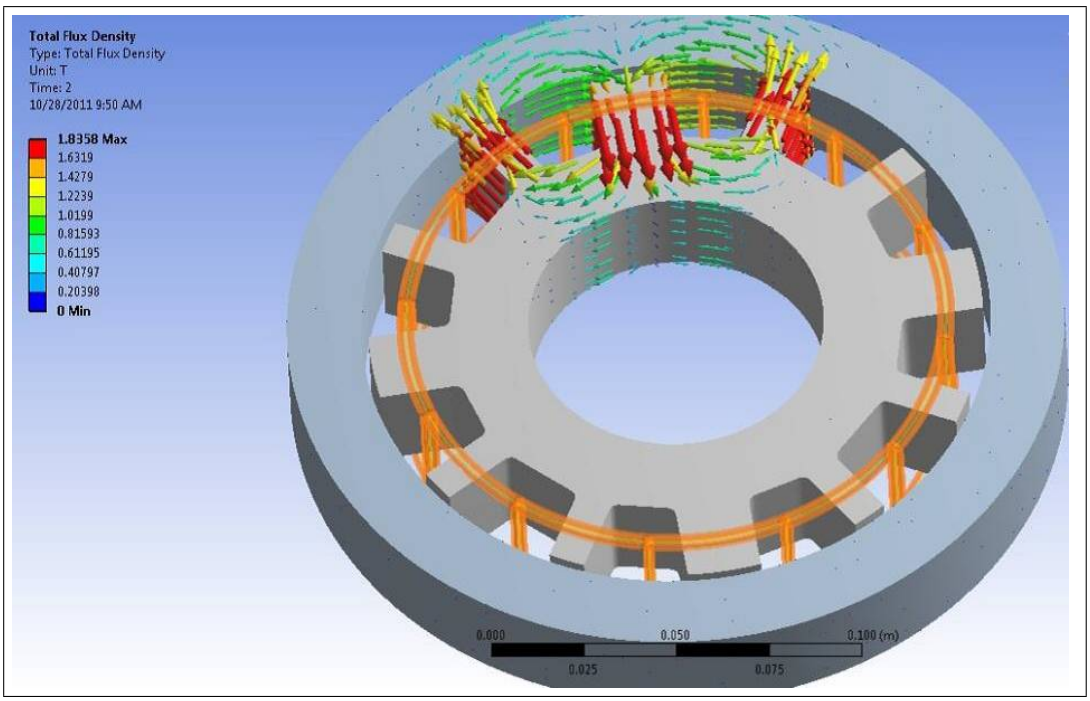

Figure 10: Radial AMB Finite Element Solution

[4] S.-M. Jang, K.-H. Kim, K.-J. Ko, J.-H. Choi, S.-Y. Sung, and Y.-B. Lee, "Improved thrust calculations of active magnetic bearings considering fringing flux," *Journal of Applied Physics*, vol. 111, no. 7, p. 07E726, 2012.

[5] M. Zhang and Y. Tian, "Frequency domain modeling of eddy current loss for magnetic thrust bearings," *Proceedings of the Institution of Mechanical Engineers, Part J: Journal of Engineering Tribology*, vol. 227, no. 7, pp. 718–728, 2013.

[6] A. Kailasan, "Preliminary Design and Analysis of an Energy Storage Flywheel," PhD Thesis, University of Virginia, Charlottesville, VA", 2013.

[7] T. W. Nehl, F. A. Fouad, and N. A. Demerdash, "Determination of saturated values of rotating machinery incremental and apparent inductances by an energy perturbation method," *IEEE Transactions on Power Apparatus and Systems*, no. 12, pp. 4441–4451, 1982.